Journal of Nuclear Materials 380 (2008) 85–92

Contents lists available at ScienceDirect

Journal of Nuclear Materials

journal homepage: www.elsevier.com/locate/jnucmat

Microstructure and thermal conductivity of Mo–TiC cermets processed by hot isostatic pressing

Marion Le Flem [a,*], Alexandre Allemand [a], Stéphane Urvoy [a], Denis Cédat [b], Colette Rey [b]

[a] CEA Saclay, DMN/SRMA, 91191 Gif-sur-Yvette cedex, France
[b] ECP, LMSSMat, Grande Voie des Vignes, 92295 Châtenay-Malabry, France

ARTICLE INFO

Article history:
Received 13 July 2007
Accepted 10 January 2008

PACS:
81.05.Mh
81.05.−t
66.30.Xj
65.40.Ba

ABSTRACT

In the scope of refractory material development for structural applications in the core of future nuclear reactors (gas fast reactors working between 500 °C and at least 800 °C in nominal conditions and up to 1650 °C in accidental scenarios), five Mo–TiC cermets, and single-phase TiC and Mo, were processed by hot isostatic pressing. Starting TiC volume contents were 0%, 12.5%, 25%, 37.5%, 50%, 75% and 100%. First, high dense specimens were characterized in terms of microstructure, composition and phase volume fractions. Cermets exhibited two phases in agreement with phase diagram previsions (Mo–$TiC_{1-2at.\%}$ and TiC–$Mo_{10-15at.\%}$), and a residual non-reacted TiC-rich phase (TiC–$Mo_{1at.\%}$). Second, heat capacity and thermal diffusivity were measured up to 1000 °C which allowed to evaluate the thermal conductivity of each cermet: this lays between TiC conductivity (12–18 W/m K) and Mo conductivity (95–125 W/m K), thermal properties continuously decreasing with starting TiC content. An analytical approach based on the volume fraction and properties of each constituent allowed to highlight the existence of thermal resistance at the interphases at low temperature.

1. Introduction

In some future nuclear reactor designs such as gas fast reactors (GFR), the core should operate at temperatures greater than 800 °C under nominal conditions and up to 1650 °C in some accident scenarios. The most promising structural materials in terms of mechanical strength at high temperature and thermal conductivity are ceramics, especially carbides such as TiC, ZrC, SiC [1–4], and refractory metallic alloys of Mo and Nb. Both types of materials exhibit major drawbacks. Monolithic ceramics show poor damage tolerance (K_{IC} = 2–5 MPa $m^{1/2}$) and are not easy to machine. Alternatively, refractory metals have large cross absorption sections which can negatively impact neutronic performance of the reactor.

Several solutions are under investigation in order to increase damage tolerance and toughness of ceramics (development of nano-grained ceramics [5], ductile ceramics [6], fiber reinforced ceramics composites...). Among them, materials combining carbide and refractory alloy are of great interest: on the one hand, toughness would be enhanced compared to monolithic carbide and, on the other hand, the neutronic penalty, depending on the total weight of refractory alloy, would be limited with regards to metallic solution.

The wide composition range for which the metal Mo/Nb and the carbide TiC/ZrC coexist [7–9] allows the balance between mechanical strength, creep resistance, ductility and toughness. Thus, lot of studies dealed with high temperature mechanical property enhancement of these cermets by adjusting carbide to ceramic volume ratio [10–21]. Most of the time, composites were produced by arc-melting [10–12,14,17], leading to more or less fine eutectic-type microstructure according to the phase diagram. Uniaxial pressing [13], pressureless sintering [18], hot isostatic pressing [19,20] and even spark plasma sintering [21] were also proposed. On a mechanical point of view, the use of Mo/Nb–TiC/ZrC composites should be consistent with the GFR design requirements. Nevertheless, whereas heat conduction properties are of major importance for such an application, no work was made to evaluate the thermal conductivity of these materials, also depending on phase volume fraction.

In this work, hot isostatic pressing (HIP) was used to densify Mo–TiC cermets in a wide composition range. The microstructure was characterized in terms of morphology, phase volume fraction and chemical composition. Finally, thermal diffusivity and specific heat of each cermet were measured to get thermal conductivity up to 1000 °C.

2. Experimental procedure

Industrial powders of Mo (Cerac, d_{50} = 5 μm) and TiC (H.C. Starck, d_{50} = 3 μm) were blended with various TiC/Mo ratio via alcoholic route. Cold isostatic pressing was used to compact the powder mixture up to 60% in relative density (250 MPa, 1 min).

* Corresponding author. Tel.: +33 (0) 1 69 08 40 98; fax: +33 (0) 1 69 08 71 30.
E-mail address: marion.leflem@cea.fr (M. Le Flem).

0022-3115/$ - see front matter © 2008 Elsevier B.V. All rights reserved.
doi:10.1016/j.jnucmat.2008.01.033

Then, the green bodies were put in a titanium can and densified by HIP during 2 h at 1600 °C under 160 MPa (solid state sintering). Single-phase Mo, single-phase TiC and five grades of Mo–TiC cermets were sintered (vol.%): Mo, Mo–TiC 12.5%, Mo–TiC 25%, Mo–TiC 37.5%, Mo–TiC 50%, Mo–TiC 75% and TiC. The compositions of the cermets lay in the two-phased domain of pseudo binary phase diagram presented in Fig. 1 [22], which shows the co-existence of the following solid solutions: TiC–$Mo_{14at.\%}$ and Mo–$TiC_{5at.\%}$. No post-sintering heat treatment was performed.

The density of each sample was measured by Archimede's method (results are presented in Table 1). The microstructure was observed by scanning electron microscopy (SEM) on polished sections (1 μm diamond). Image analysis was performed on the micrographs to precise the phase proportion and the composition was examined in a microprobe analyser by wavelength dispersive spectroscopy (WDS). Micro-hardness tests were carried out on each sample with a 300 g-loading Vickers micro-indenter and Young modulus was measured by impulse excitation technique at room temperature.

Thermal conductivity λ was calculated between room temperature and 1000 °C from diffusivity and heat capacity measurements using the following formula:

$$\lambda(\mathrm{W/m\,K}) = C_p \times \alpha \times \rho \quad (1)$$

with a the thermal diffusivity (mm^2/s), C_p the heat capacity (J/g K) and ρ the geometric density. C_p was determined in argon between room temperature and 800 °C and the laser-flash method (laser Nd–Phosphate) was used to measure the thermal diffusivity a in helium up to 1273 K, taking into account thermal loss as described in [23].

Table 1
Cermet density

Grade (vol.%)	Density
Mo 100%	10.0
Mo–TiC 12.5%	9.5
Mo–TiC 25%	8.7
Mo–TiC 37.5%	8.1
Mo–TiC 50%	7.4
Mo–TiC 75%	6.0
TiC 100%	4.9

3. Microstructure

SEM micrographs of Mo–TiC cermets are presented in Fig. 2. The samples are cohesive, crack free and exhibit very small residual porosity in agreement with the high measured densities. Three phases are systematically observed, which proportions depend on starting TiC/Mo ratio. WDS analysis allowed to evaluate the chemical composition of each phase, which does not depend on the cermet grade:

- light 'Mo-phase': Mo–$TiC_{1-2at.\%}$
- dark 'TiC-phase': TiC–$Mo_{1at.\%}$

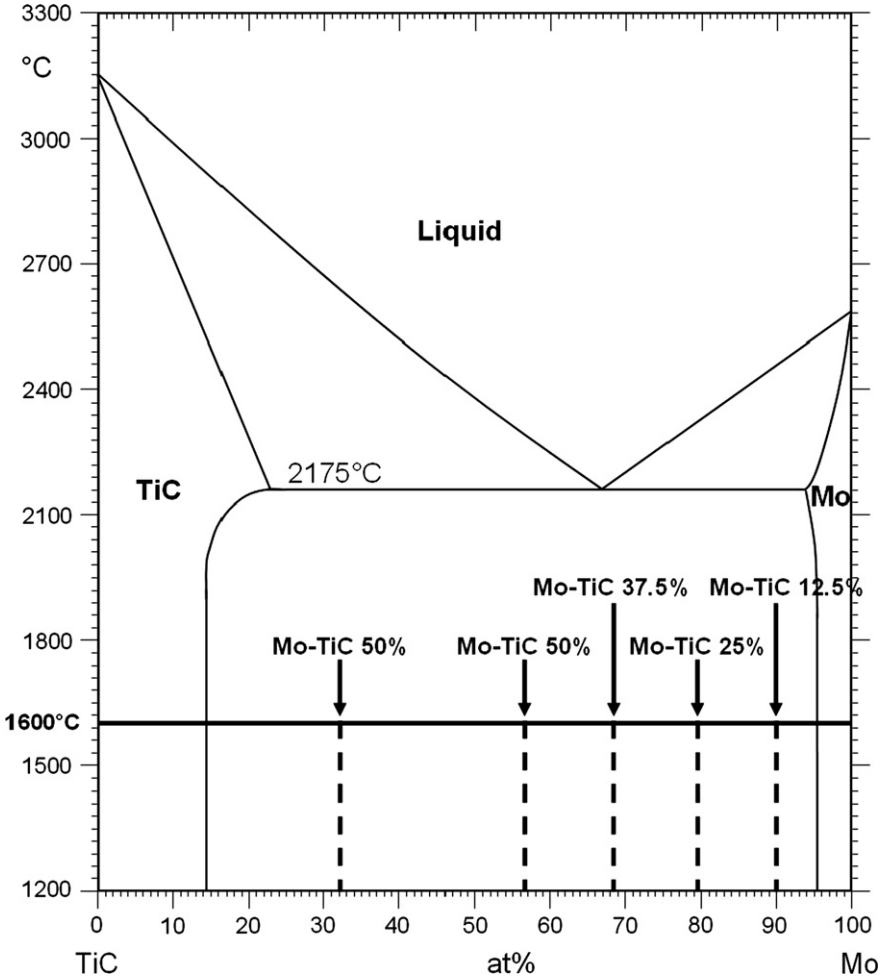

Fig. 1. Pseudo-binary Mo–TiC phase diagram [22]. Investigated cermet compositions are reported.

- gray mixed-carbide, located at the interfaces: TiC–$Mo_{10-15.at\%}$ phase.

It seems obvious that Mo–$TiC_{1-2.at\%}$ phase and TiC–$Mo_{1.at\%}$ phase correspond to former Mo and TiC particles; some agglomerates are clearly visible (arrowed in Fig. 2c); the gray phase results from interdiffusion between TiC and Mo (XRD confirmed that no Mo_2C was formed).

The compositions are in quite good agreement with phase diagram predictions: Mo–$TiC_{1-2at.\%}$ versus expected Mo–$TiC_{5at.\%}$ and TiC–$Mo_{10-15at.\%}$ versus expected TiC–$Mo_{14at.\%}$. The slight discrepancy can be explained by the presence of oxygen as pollution in the starting powder, which should affect the equilibrium compositions and the solubility domains. Oxygen distribution is the following (WDS analysis): 1–2at.% in Mo-phase, 2.5–3.5at.% in the mixed-carbide and up to 5% in TiC-phase. The high pollution of TiC-phase is due to the large affinity of oxygen for carbide especially during high temperature processing. Anyway, the TiC-phase can be considered as a non-equilibrium residual phase. Its presence should be linked to the HIP method used to sinter the composite, high pressure involving shift of transformation points to higher temperatures with respect to thermodynamic predictions. Fine microstructure observations obtained by transmission electron microscopy (TEM) are detailed elsewhere [24].

In order to precise the proportion of each phase, which evolves with the starting TiC/Mo ratio, image analysis based on gray levels was achieved on several SEM micrographs of each cermet. Because HIP is an isotropic process leading to isotropic microstructures, the surface proportions were assumed to be representative of the volume proportions. Results are presented in Table 2 and in Fig. 3 versus the starting amount of TiC and Mo powder. Fig. 3a shows that the metal proportion is kept in the final material (from Mo to Mo-phase), i.e. the diffusion of Ti and C in Mo particles, to reach the composition Mo–$TiC_{1-2at.\%}$, did not involve any significant volume change in this composition range. Otherwise, the TiC-phase proportion is much lower than the starting TiC amount, particularly for high TiC content where the discrepancy is as high as 60% (for Mo–TiC 75%). This suggests that TiC particles have been consumed by Mo diffusion during the high temperature sintering. Thus, the cermet can be considered as a composite material with (i) a metallic phase, Mo-phase, which volume fraction matches quite well with the starting Mo proportion, and (ii) a ceramic phase, 'TiC-phase + mixed-carbide', which volume fraction corresponds to the starting TiC proportion as shown in Table 2.

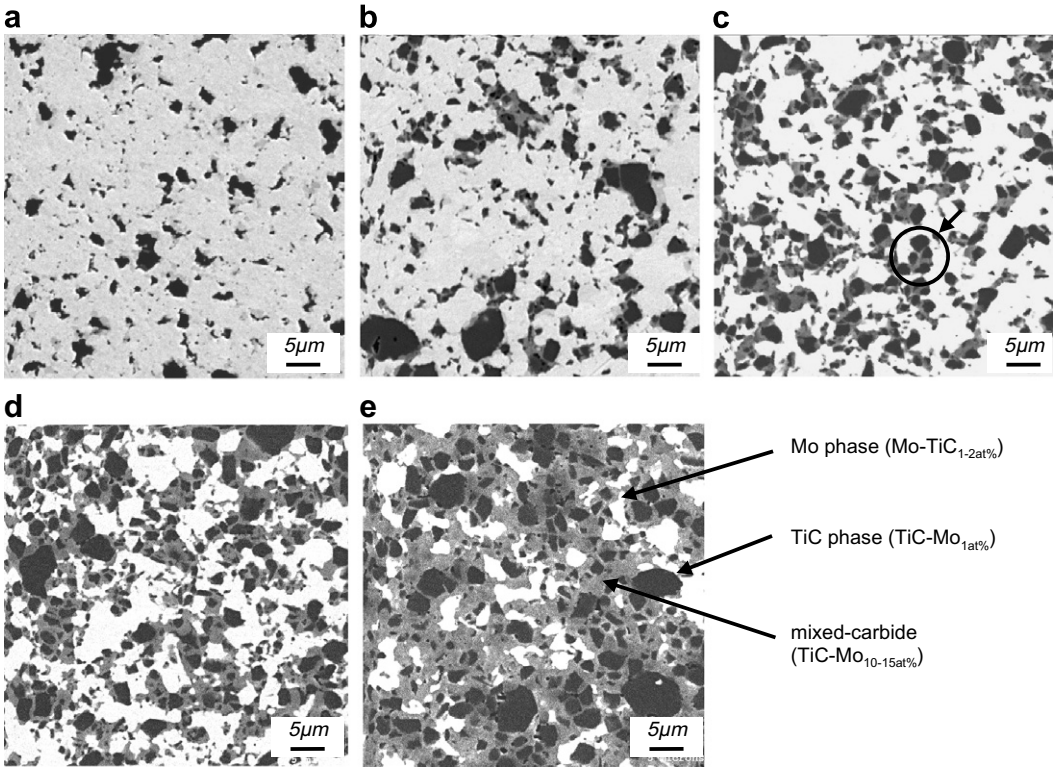

Fig. 2. SEM micrographs of (a) Mo–TiC 12.5%, (b) Mo–TiC 25%, (c) Mo–TiC 37.5%, (d) Mo–TiC 50%, (e) Mo–TiC 75%.

Table 2
Phase proportion in cermet determined by image analysis

	Volume fraction (%)			
	Metallic phase (Φ_{met})	Ceramic phase (Φ_{ceram})		
	Mo-phase	TiC-phase	Mixed carbide	TiC-phase-phase + mixed carbide
Mo–TiC 12.5%	82	8	10	18
Mo–TiC 25%	78	11	11	22
Mo–TiC 37.5%	59	19	22	41
Mo–TiC 50%	50	21	29	50
Mo–TiC 75%	18	29	53	82

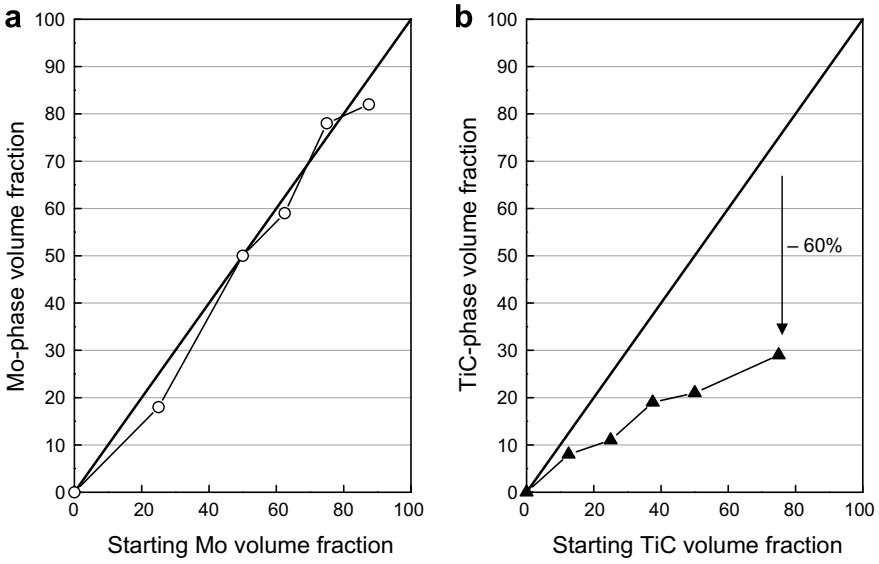

Fig. 3. (a) Mo-phase and (b) TiC-phase volume fraction versus starting Mo and TiC volume fraction.

This diffusion of Mo in TiC particles is also suggested by the microstructure of the cermets. Indeed, the TiC-phase exists as agglomerates of former TiC particles that are embedded in the gray mixed-carbide (arrowed in Fig. 2c). The mechanism could be the following: since the melting temperature of TiC is higher than the melting temperature of Mo (T_m(TiC) ~ 3100 °C while T_m(Mo) ~ 2610 °C), the diffusion of Mo should happen first, i.e. during the early step of sintering, and especially at boundaries of TiC particles for which bridging is not effective yet.

4. Micro-hardness, Young modulus

Hardness, measured by indentation, and Young modulus, measured by impulse excitation technique, were determined on every cermet specimen as well as for single-phase Mo and single-phase TiC samples. The changes in hardness and Young modulus are presented in Fig. 4 versus starting TiC content. Both exhibit a progressive increase with TiC content, i.e. with ceramic phase content, consistent with the properties of single-phase Mo (H = 2.5 GPa, E = 327 GPa) and single-phase TiC (H = 22 GPa, E = 440 GPa). Unfortunately, the indentation cracks generated from indentation prints did not fit the conditions required to estimate K_{IC}. Nevertheless, toughness could be estimated at 8.8 MPa$\sqrt{m}$ for Mo–TiC 50% sample. This is in relative agreement with results on hot pressed and thermal annealed Mo–TiC cermets (about 6.5 MPa$\sqrt{m}$) [13] and on arc-melted and thermal annealed Nb–ZrC cermets (about 7.5 MPa$\sqrt{m}$) [14], both for equivalent starting metal to carbide ratio (toughness obtained by three-point bending tests on single-edge notched beams).

5. Thermal conductivity

The heat capacity C_p and the thermal diffusivity a were measured on each cermet and on the single-phase Mo and the single-phase TiC specimens. The results are presented versus temperature in Fig. 5(a) and (b). C_p and a values range from TiC characteristics to Mo characteristics with increasing starting TiC proportion (except for the diffusivity of Mo–TiC 75% which is a bit lower than TiC diffusivity). Their dependence with respect to the temperature can be described using the following formula: $A + B \cdot (\theta + 273) + C \cdot (\theta + 273)^2 + D/(\theta + 273)^2$, available up to 800 °C for C_p (Table 3) and 1000 °C for a (Table 4). One can notice that using C_p of single-phase Mo and single-phase TiC in the proportion of the metallic phase and ceramic phase (see Table 2) allows a quite good estimation of the experimental C_p.

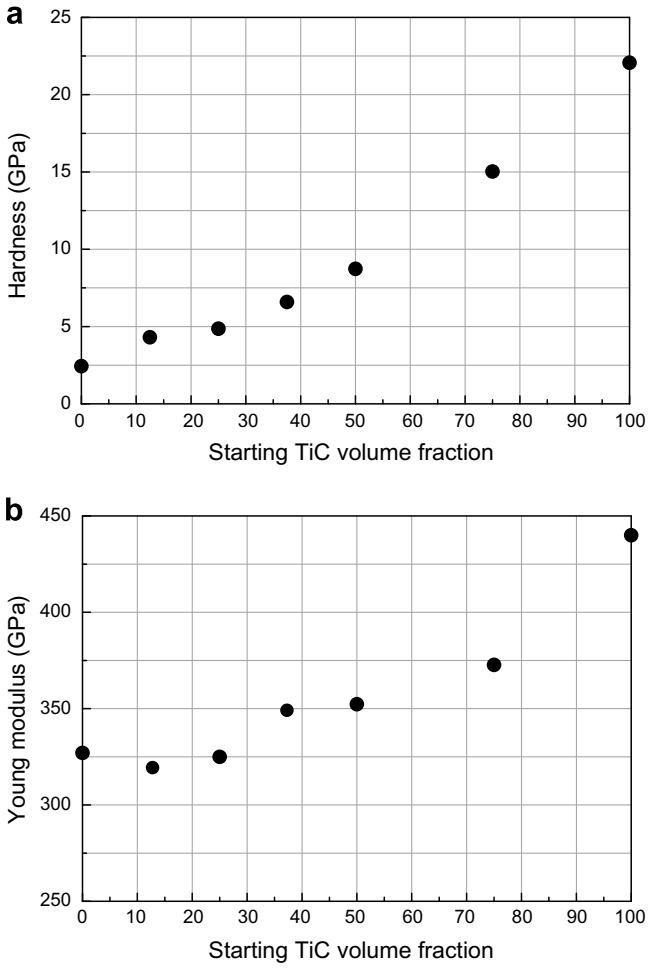

Fig. 4. Hardness and Young modulus of cermets versus starting TiC volume fraction.

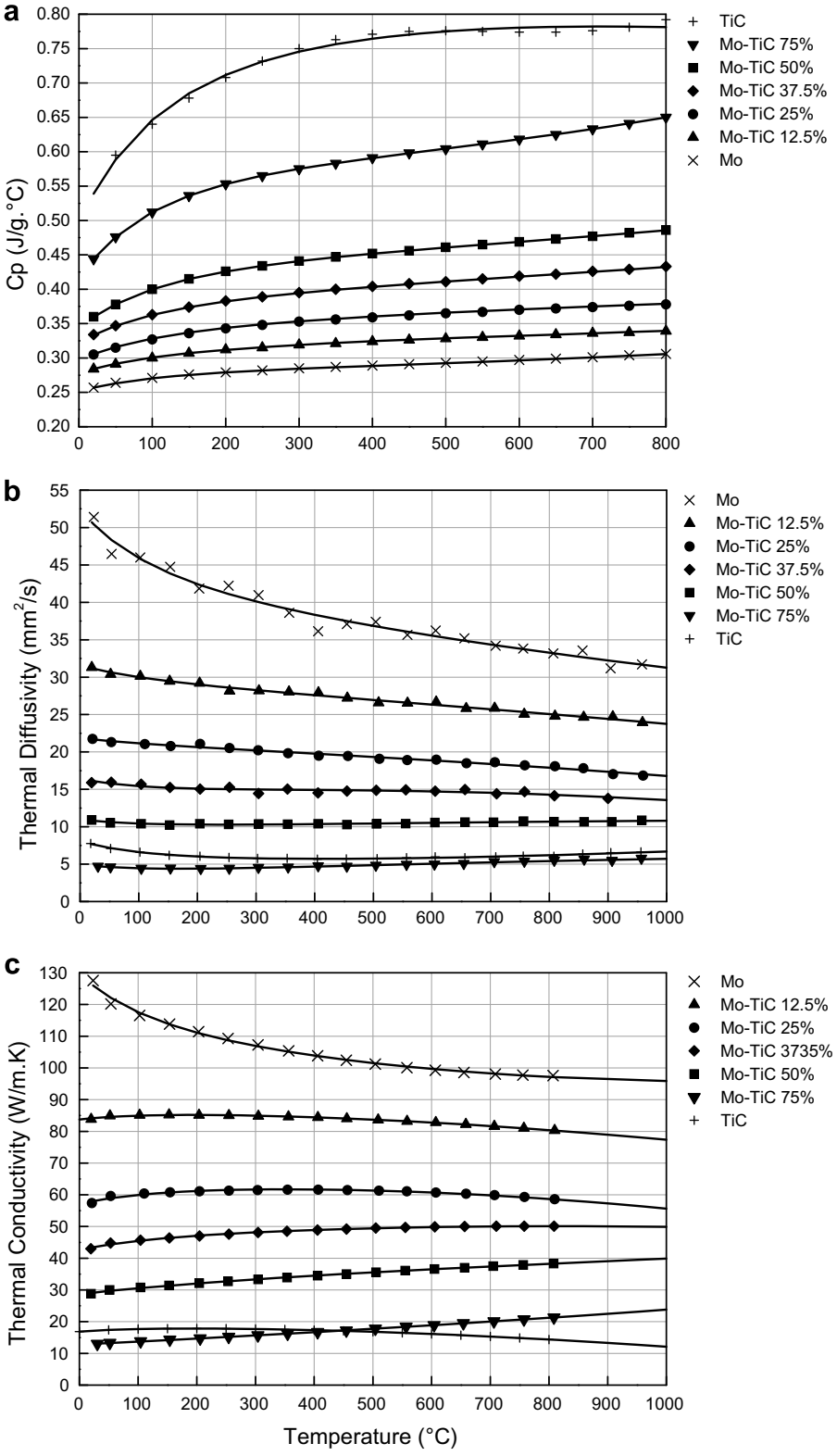

Fig. 5. (a) Heat capacity C_p, (b) thermal diffusivity a and (c) thermal conductivity λ of cermets versus temperature.

The thermal conductivity λ was then calculated from C_p and a and from the geometric density ρ (equal to 5.86). Its evolution is presented in Fig. 5c between room temperature and 1000 °C and can be fitted up to 1000 °C with the same formula as for C_p and a (Table 5). The thermal conductivity of Mo-TiC cermets is quite constant up to 1000 °C. As specific heat and thermal diffusivity, it lays between Mo and TiC characteristics, exhibiting a progressive evolution with the starting TiC content (decrease in conductivity). The conductivity of Mo–TiC 75% and single-phase TiC are very close and, considering experimental discrepancy, can be considered as similar.

Table 3
Adjusted parameters for C_p change versus temperature θ (20–800 °C)

	C_p (J/g K) = $A + B\cdot(\theta+273) + C\cdot(\theta+273)^2 + D/(\theta+273)^2$			
	A	B	C	D
Mo	0.298	-2.457×10^{-5}	3.273×10^{-8}	-3.066×10^{3}
Mo–TiC 12.5%	0.317	1.833×10^{-5}	0.490×10^{-8}	-3.314×10^{3}
Mo–TiC 25%	0.347	3.345×10^{-5}	-0.097×10^{-8}	-4.460×10^{3}
Mo–TiC 37.5%	0.400	0.848×10^{-5}	2.486×10^{-8}	-6.114×10^{3}
Mo–TiC 50%	0.466	-2.219×10^{-5}	4.457×10^{-8}	-8.906×10^{3}
Mo–TiC 75%	0.673	-16.877×10^{-5}	14.974×10^{-8}	-16.498×10^{3}
TiC	0.803	5.744×10^{-5}	-5.427×10^{-8}	-23.685×10^{3}

Table 4
Adjusted parameters for a change versus temperature θ (20–1000 °C)

	$\alpha(\mathrm{mm^2/s}) = A + B\cdot(\theta+273) + C\cdot(\theta+273)^2 + D/(\theta+273)^2$			
	A	B	C	D
Mo	44.144	-12.504×10^{-3}	1.548×10^{-6}	8.664×10^{5}
Mo–TiC 12,5%	30.342	-4.036×10^{-3}	-0.960×10^{-6}	1.805×10^{5}
Mo–TiC 25%	21.538	-1.824×10^{-3}	-1.525×10^{-6}	0.704×10^{5}
Mo–TiC 37.5%	11.858	6.654×10^{-3}	-4.261×10^{-6}	2.322×10^{5}
Mo–TiC 50%	8.679	2.625×10^{-3}	-0.803×10^{-6}	1.230×10^{5}
Mo–TiC 75%	2.015	4.210×10^{-3}	-1.081×10^{-6}	1.411×10^{5}
TiC	4.700	-0.161×10^{-3}	1.256×10^{-6}	2.496×10^{5}

Table 5
Adjusted parameters for λ change versus temperature θ (20–1000 °C)

	$\lambda(\mathrm{W/m\ K}) = A + B\cdot(\theta+273) + C\cdot(\theta+273)^2 + D/(\theta+273)^2$			
	A	B	C	D
Mo	116.486	-3.161×10^{-2}	11.495×10^{-6}	15.686×10^{5}
Mo–TiC 12.5%	86.757	0.248×10^{-2}	-7.666×10^{-6}	-2.329×10^{5}
Mo–TiC 25%	60.331	1.093×10^{-2}	-11.322×10^{-6}	-4.000×10^{5}
Mo–TiC 37.5%	44.238	1.180×10^{-2}	-5.648×10^{-6}	-3.318×10^{5}
Mo–TiC 50%	27.243	1.259×10^{-2}	-2.048×10^{-6}	-1.468×10^{5}
Mo–TiC 75%	11.046	0.666×10^{-2}	2.648×10^{-6}	-0.238×10^{5}
TiC	18.615	0.264×10^{-2}	-6.032×10^{-6}	-1.508×10^{5}

Plotting conductivity change with ceramic volume fraction allows to highlight changes with cermet composition, as shown in Fig. 6. Whatever the considered temperature, thermal conductivity drops when a small amount of TiC is added to Mo. Thus, low conductivity of TiC, regarding high conductivity of Mo, induces a strong penalty in terms of thermal properties. Beyond a starting TiC content of 50%, the thermal conductivity is very comparable to TiC: this could be explained by the percolation of the carbide ceramic phase in the cermet, giving the material characteristics of TiC.

Many models aim to forecast the thermal properties of a two-phase-material from the characteristics of each constituent and their volume fractions [25]. Limiting parameters are those linked to morphology, distribution and contact of the phases because they are quite uneasy to describe: independent spheres [26], interconnected spheres [27], geometric aspect ratio [28], etc. Commonly, the experimental conductivity of a two-phase-material lies between the arithmetic average (linear):

$$\lambda_{\mathrm{arithm}} = \lambda_1\cdot\Phi + \lambda_2.(1-\Phi) \tag{2}$$

and the geometric average:

$$\lambda_{\mathrm{geom}} = \lambda_1^{\Phi}\times\lambda_2^{(1-\Phi)} \tag{3}$$

with λ_1 and Φ the conductivity and volume fraction of the dispersed phase and λ_2 the matrix conductivity.

The following expression reported by [29] is said to be quite representative of a microstructure of randomly dispersed particles existing both as individual particle and in a 3D interconnected network:

$$\lambda_{\mathrm{eff}} = \frac{1}{4}\Big[(2-3\cdot\Phi)\lambda_2 + (3\cdot\Phi-1)\lambda_1 + \sqrt{8\lambda_1\lambda_2 + ((2-3\cdot\Phi)\lambda_2 + (3\cdot\Phi-1)\lambda_1)^2}\Big] \tag{4}$$

These three formulas were used to evaluate the thermal conductivity of the three-phase-Mo–TiC cermets, considering a two-phase-material with (i) a metallic phase and (ii) a ceramic phase, and according to the following hypothesis:

- The conductivity of metallic phase, i.e. Mo-phase (Mo–$TiC_{1at.\%}$), is the conductivity of single-phase Mo (with volume fraction Φ_{met} from Table 2).
- The conductivity of ceramic phase, i.e. both TiC-phase (TiC–$Mo_{1at.\%}$) and mixed-carbide (TiC–$Mo_{10-15at.\%}$), is assimilated to the conductivity of single-phase TiC (with volume fraction Φ_{ceram} from Table 2).
- Porosity is zero.
- Thermal resistance at interfaces is zero.

The experimental and calculated evolutions of conductivity versus the ceramic phase volume fraction Φ_{ceram} are presented in Fig. 6 at 20 °C, 500 °C and 1000 °C. At 20 °C, the calculations systematically over-estimate the experimental conductivity. Regarding the microstructure of the cermet (lot of interfaces), the thermal resistance effect should exist and, among all the

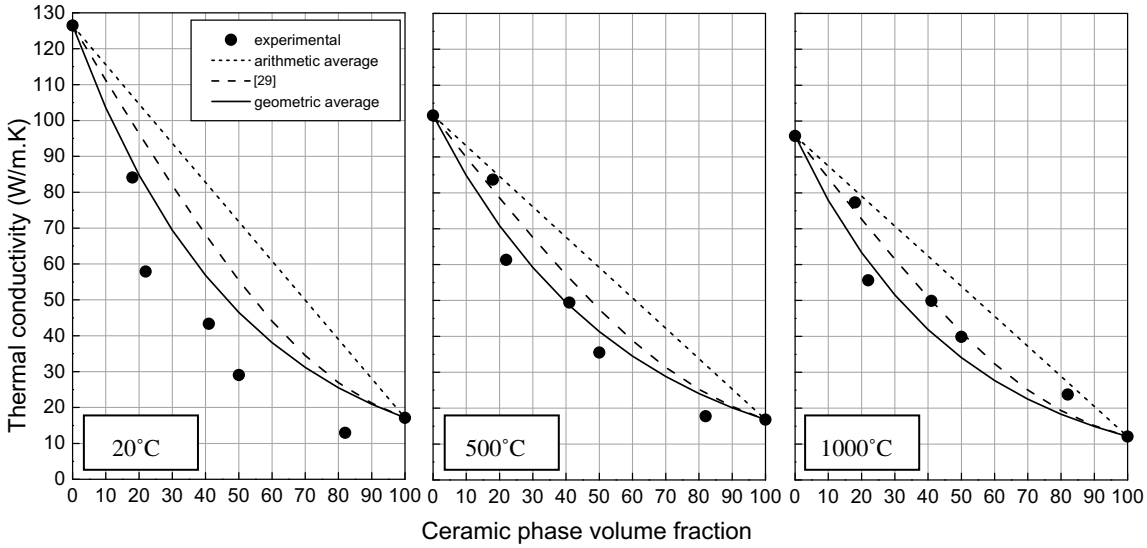

Fig. 6. Evolution of thermal conductivity at 20 °C, 500 °C and 1000 °C.

hypothesis, could reasonably explain such a discrepancy. However, this last seems to be reduced with increasing temperature: thus, at 1000 °C, almost all the experimental plots lay between arithmetic average and geometric average estimations, being quite consistent with the predictions from [29]. This suggests the thermal resistance at the interfaces is lowered by higher temperature; the origin could be the thermal expansion of the phases, allowing a better contact at the interfaces and then decreasing the interfaces thermal resistance (α(TiC) = $7.8{\cdot}10^{-6}$/°C, α(Mo) = $4.8{\cdot}10^{-6}$/°C).

6. Conclusion

Hot isostatic pressing allowed to fabricate high densified and crack-free Mo–TiC cermets for a wide composition range. Samples exhibited three phases: two of them were close to the thermodynamic predictions (Mo-phase: Mo–$TiC_{1-2\ at.\%}$ and mixed-carbide: TiC–$Mo_{10-15at.\%}$), and one was a residual phase corresponding to non-reacted TiC (TiC–$Mo_{1at.\%}$). Unfortunately, an oxygen pollution occurred which should have lead to composition shift regarding phase diagram predictions.

Heat capacity and thermal diffusivity measurements allowed to calculate thermal conductivity up to 1000 °C. Thermal conductivity is quite constant with temperature, but continuously decreases with increasing ceramic phase content from the conductivity of the single-phase Mo down to the conductivity of single-phase TiC. Calculations, based on thermal properties of single-phase Mo and single-phase TiC and their respective volume fractions, tended to overestimate the experimental values at low temperature but were quite consistent with measurements upon 500 °C. The role of thermal resistance at the interfaces was highlighted. Thermal resistance leads to a decrease in conductivity at low temperature but seems weaker at higher temperature: the role of thermal expansion of the constituents allowing a better contact between the phases was suggested. Anyway, the thermal properties of Mo–TiC cermets are in agreement with the specifications required in the scope of GFR design.

To estimate the stability of these cermets with respect to temperature in terms of microstructure and thermal properties, thermal annealing will be performed at temperatures representative of in-service conditions. In addition, other densification processes will be explored, such as extrusion, more adapted to industrial fabrication of high amount of materials (cladding tubes for instance). Finally, investigations of mechanical properties are in progress, in particular to precise the accommodation of deformation at interphases [30].

Aknowledgements

Authors would like to thank Ms Céline Chan, Mr Marc Scolan and Mr Cyril Gaudillère for their contribution to this work through their trainees. Mr Gilles Vaux who made cermet sintering and Mr Didier Hamon who performed WDS analysis are also thanked. Finally, authors are very grateful to Mr Etienne Castelier for discussions about thermal conductivity of cermets materials.

References

[1] M. Dormeval, J.L. Séran, D. Gosset, P. Wident, A. Allemand, J. Canel, F. Ravel, Ph. Billot, in: Proceedings of ICAPP '05, 15–19 May 2005, Seoul, Korea.
[2] M. Le Flem (Dormeval), A. Allemand, in: Proceedings of Sintering 2005, 29 August–1 September 2005, Grenoble, France.
[3] A. Allemand, M. Le Flem, F. Guillard, in: Proceedings of Sintering 2005, 29 August–1 September 2005, Grenoble, France.
[4] M. Le Flem, A. Allemand, S. Urvoy, J.L. Séran, in: Proceedings of HTR2006: Third International Topical Meeting on High Temperature Reactor Technology, 1–4 October 2006, Johannesburg, South Africa.
[5] C. Mengeot, B. Guizard, S. Poissonnet, L. Boulanger, M. Le Flem, F. Guillard, F. Ténégal, Matériaux et Techniques 95 (2007) 289.
[6] F. Barcelo, S. Doriot, T. Cozzika, M. Le Flem, J.L. Béchade, M. Radovic, M.W. Barsoum, in: Proceedings of the 31st International Conference on Advanced ceramics and Composites, 21–26 January 2007, Daytona Beach, USA.
[7] P. Stecher, F. Benesovsky, A. Neckel, H. Nowotny, Monatsh. Chem. 95 (1964) 1360.
[8] K. One, J. Moriyama, Handbook of Ternary Alloy phase Diagrams, vol. 6, American Society for Metals, Materials Park, OH, 1995. p. 7200.
[9] H.N. Eremenko, Handbook of Ternary Alloy phase Diagrams, vol. 6, American Society for Metals, Materials Park, OH, 1995.
[10] T. Suzuki, N. Nomura, K. Yoshimi, S. Hanada, Mat. Trans. JIM 41 9 (2000) 1164.
[11] T. Suzuki, H. Matsumoto, N. Nomura, S. Hanada, Sci. Tech. Adv. Mater. 3 (2002) 137.
[12] T. Suzuki, H. Matsumoto, N. Nomura, S. Hanada, Mater. Trans. 41 (2000) 1164.
[13] N. Nomura, K. Yoshimi, S. Hanada, Mat. Trans. JIM 41 12 (2000) 1599.
[14] Y. Tan, C.L. Ma, A. Kasama, R. Tanaka, Y. Mishima, S. Hanada, J.M. Yang, Mater. Sci. Eng. A 341 (2003) 282.
[15] Y. Tan, C.L. Ma, A. Kasama, R. Tanaka, S. Hanada, J.M. Yang, Mater. Sci. Eng. A 355 (2003) 260.
[16] T. Takida, M. Mabuchi, T. Igarashi, Y. Doi, T. Nagae, Mater. Sci. Eng. A 276 (1–2) (2000) 269.
[17] N. Nomura, K. Yoshimi, T. Konno, S. Hanada, J. Mater. Sci. Lett. 19 (2000) 1879.
[18] S.E. Landwehr, G.E. Hilmas, W.G. Fahrenholtz, I.G. Talmy, J. Am. Soc. 91 (3) (2008) 873.
[19] H. Kurishita, Y. Kitsuanai, T. Shibatama, H. Kayano, U. Hiraoka, JNM 233–237 (1996) 557.

[20] T. Takida, T. Igarashi, Y. Doi, H. Hiraika, J. Jpn. Soc. Powder Powder Metall. 45 (1998) 974.
[21] T. Takida, M. Mabuchi, M. Nakamura, T. Igarashi, Y. Doi, T. Nagae, Mater. Sci. Eng. 276 (2000) 269.
[22] H.N. Eremenko, Handbook of Ternary Alloy Phase Diagrams, vol. 6, American Society for Metals, Materials Park, OH, 1995. 7089.
[23] D. Gosset, M. Colin, High Temperatures – High pressures 34 (2002) 265.
[24] D. Cédat, C. Rey, M. Clavel, J.H. Schmitt, M. Le Flem, A. Allemand, J. Nucl. Mater., accepted for publication.
[25] I.V. Belova, G.E. Murch, J. Mater. Process Technol. 153–154 (2004) 741.
[26] J.C. Maxwell, Treatise on Electricity and Magnetism, vol. 1, Clarendon, Oxford, 1982.
[27] K.J. Singh, R. Singh, D.R. Chaudhary, J. Phys. D: Appl. Phys. 31 (1998) 1681.
[28] L.S. Verma, A.K. Shrotriya, R. Singh, D.R. Chaudhary, J. Phys. D: Appl. Phys. 24 (1991) 1729.
[29] A.D. Brailsford, K.G. Major, Br. J. Appl. Phys. 15 (1964) 313.
[30] D. Cédat, C. Rey, M. Clavel, J.H. Schmitt, M. Le Flem, A. Allemand, Characterisation for numerical study of mechanical behaviour of cermet Mo–TiC, in: E. Cueto, F. Chinesta (Eds.), AIP Proceeding of the 10th ESAFORM Conference on Material Forming, April 18–20 2007, 907, American Institute of Physics, Zaragoza, Spain, 2007.